Ultrasound in Med. & Biol., Vol. 36, No. 5, pp. 733–742, 2010

0301-5629/$–see front matter

ELSEVIER

doi:10.1016/j.ultrasmedbio.2010.02.006

● *Original Contribution*

HIGH-RESOLUTION PHOTOACOUSTIC IMAGING OF OCULAR TISSUES

RONALD H. SILVERMAN,*† FANTING KONG,‡ Y. C. CHEN,‡ HARRIET O. LLOYD,* HYUNG HAM KIM,§ JONATHAN M. CANNATA,§ K. KIRK SHUNG,§ and D. JACKSON COLEMAN*

*Department of Ophthalmology, Weill Cornell Medical College, New York, NY, USA; †F.L. Lizzi Center for Biomedical Engineering, Riverside Research Institute, New York, NY, USA; ‡Department of Physics and Astronomy, Hunter College, City University of New York, New York, NY, USA; and §Department of Biomedical Engineering, University of Southern California, Los Angeles, CA, USA

(*Received* 5 *January* 2009; *revised* 28 *January* 2010; *in final form* 11 *February* 2010)

Abstract—Optical coherence tomography (OCT) and ultrasound (US) are methods widely used for diagnostic imaging of the eye. These techniques detect discontinuities in optical refractive index and acoustic impedance, respectively. Because these both relate to variations in tissue density or composition, OCT and US images share a qualitatively similar appearance. In photoacoustic imaging (PAI), short light pulses are directed at tissues, pressure is generated due to a rapid energy deposition in the tissue volume and thermoelastic expansion results in generation of broadband US. PAI thus depicts optical absorption, which is independent of the tissue characteristics imaged by OCT or US. Our aim was to demonstrate the application of PAI in ocular tissues and to do so with lateral resolution comparable to OCT. We developed two PAI assemblies, both of which used single-element US transducers and lasers sharing a common focus. The first assembly had optical and 35-MHz US axes offset by a 30° angle. The second assembly consisted of a 20-MHz ring transducer with a coaxial optics. The laser emitted 5-ns pulses at either 532 nm or 1064 nm, with spot sizes at the focus of 35 μm for the angled probe and 20 μm for the coaxial probe. We compared lateral resolution by scanning 12.5 μm diameter wire targets with pulse/echo US and PAI at each wavelength. We then imaged the anterior segment in whole *ex vivo* pig eyes and the choroid and ciliary body region in sectioned eyes. PAI data obtained at 1064 nm in the near infrared had higher penetration but reduced signal amplitude compared to that obtained using the 532 nm green wavelength. Images were obtained of the iris, choroid and ciliary processes. The zonules and anterior cornea and lens surfaces were seen at 532 nm. Because the laser spot size was significantly smaller than the US beamwidth at the focus, PAI images had superior resolution than those obtained using conventional US. (E-mail: rsilverman@rri-usa.org)

Key Words: **Ultrasound, Photoacoustic, Eye, Imaging, Ophthalmology.**

INTRODUCTION

Ultrasound (US) and optical coherence tomography (OCT) each play an invaluable role in diagnostic imaging of the eye. In high-resolution ophthalmic US (Ishikawa and Schulman 2004; Silverman 2009), a focused high-frequency acoustic pulse emitted by the piezoelectric element of the transducer propagates through tissue and reflections are produced where the US wave encounters acoustic impedance (density x speed-of-sound) discontinuities. The time delay to each reflection detected by the transducer is proportional to range. In OCT (Drexler and Fujimoto 2008; Huang et al. 1991), a low-coherence light beam is split into reference (mirror) and sample (tissue) paths and then recombined interferometrically to allow detection of optical backscatter along the sample path as a function of range. Optical backscatter results from the presence of refractive index discontinuities, which in soft tissues may include connective tissues, cytoplasmic organelles, cell nuclei and melanin granules (Tuchin 2007), structural elements that may also produce acoustic backscatter, especially at higher frequencies. Despite their differences and the higher resolution of OCT, there is a remarkable similarity in the qualitative appearance of ultrasound biomicroscopy (UBM) and OCT images because discontinuities in tissue density are the source of backscatter in both cases. Diagnostic imaging would benefit from the use of multiple imaging modes depicting independent tissue properties. In this report, we describe

Address correspondence to: Ronald H. Silverman, Ph.D., Department of Ophthalmology, Weill Cornell Medical College, 1300 York Ave., Room LC303,New York, NY 10065. E-mail: rsilverman@rri-usa.org

the use of high-resolution photoacoustic imaging (also known as optoacoustic imaging), a modality that meets this criterion in respect to both US and OCT.

In photoacoustic imaging (PAI) (Oraevsky et al. 1993, 1994; Kruger 1994; Xu and Wang 2006; Oraevsky and Karabutov 2003), absorption of a short light pulse by chromophores present in a tissue results in local tissue volume expansion, generation of a pressure gradient and outward propagation of broadband ultrasound. The magnitude of this PAI signal is proportional to local fluence and the optical absorption coefficient of the illuminated tissue at the wavelength of the light source. Hence, images produced by this method represent optical absorption, a parameter that is independent of those depicted by US or OCT. Because optical absorption may take place with either ballistic or scattered photons and because acoustic scattering is far less than optical scattering, PAI can image deeper into tissue than can OCT, which is degraded by optical scattering.

To attain a given spatial resolution with PAI, light pulse duration must be shorter than the thermal and stress confinement traversal times for a region of the desired resolution dimension (Oraevsky et al. 1993). Because thermal diffusion is several orders of magnitude slower than stress (pressure) relaxation, the latter parameter determines resolution. However, the actual axial and lateral resolution obtained with a PAI system is limited by the bandwidth and focal properties of the US transducer used to detect the PAI signal. Because the detected broadband PAI signal is convolved with the impulse response of the transducer, resolution is limited to $c/\triangle f$, where c is the speed of sound and $\triangle f$ represents bandwidth. PAI is somewhat advantageous compared with pulse/echo ultrasound in this respect because the higher frequency components of the broadband photoacoustic signal suffer relatively less attenuation as they traverse intervening tissues in only one direction.

For PAI performed with an unfocused light source, lateral resolution simply corresponds to the beamwidth of the ultrasound transducer. If, however, the laser spot size is smaller than the acoustic beamwidth, lateral resolution will be superior to that obtained with an unfocused laser to a tissue depth such that optical scattering causes the laser beam diameter to spread to that of the ultrasound beamwidth. Maslov et al. for example, demonstrated use of a focused laser for PAI of superficial subcutaneous capillaries in mice (Maslov et al. 2008).

The eye, shown schematically in Figure 1, is unique in offering optical access to internal structures such as the retina via the cornea, crystalline lens, the fluid-filled anterior chamber and the gel-like vitreous all of which (in healthy eyes) have low absorption and negligible light scattering. The superficiality of ocular tissues confers some advantage to focusing. The mean free path of transport (the mean distance between photon scatterings) at 633 nm for the retina, the retinal pigment epithelium and the choroid are reported to be 1 mm, 10 μm and 86 μm, respectively (Hammer et al. 1995; Rovati et al. 2007). Because the retinal mean free path of transport exceeds retinal thickness (about 0.25 mm in humans), OCT, which relies on ballistic photons, can image the retina with great success. Hence, the use of a focused pulsed laser will be advantageous for PAI imaging of this tissue and possibly the underlying choroid as well. By focusing the laser, lateral resolution comparable to OCT (on the order of 10 μm) may be achievable and this may well be a requirement for clinical relevance and acceptance. Furthermore, focusing allows use of a lower power laser since only a tiny spot is illuminated.

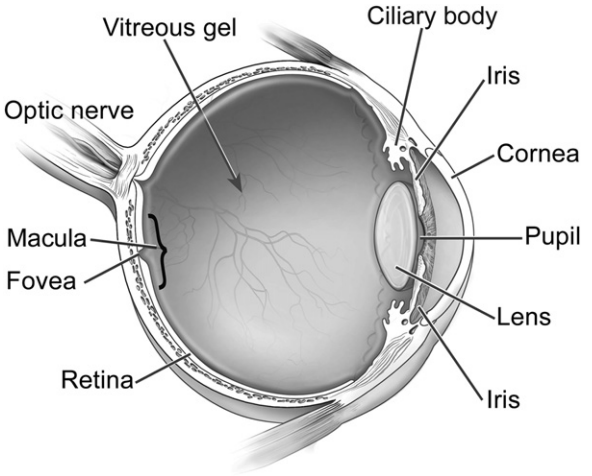

Fig. 1. Schematic drawing of eye. (Courtesy of National Eye Institute).

The major light-absorbing biomolecules in the eye are melanin and hemoglobin. Melanin, present in the uvea (iris, choroid, ciliary body) and in pigmented tumors, has maximum absorption in the ultraviolet, decreasing monotonically through the visible to the near infrared (NIR) (Sardar et al. 2001). Hemoglobin, present in the rich microvasculature of the uveal tract, in other superficial microvessels of the eye (retina, conjunctiva) and in pathologic neovascularization (including tumors), has peak absorption at around 580 nm but with distinct differences between oxy- and deoxy-hemoglobin, *e.g.*, with the former peaking broadly in the NIR at approximately 1 μm and the latter near 757 nm (Wray et al. 1988).

PAI and US imaging can be performed simultaneously, since the US transducer can operate in either pulse/echo mode or receive only mode (for PAI). This provides a mechanism for imaging of two independent tissue characteristics: acoustic impedance discontinuity and optical absorption (Emelianov et al. 2004). Furthermore, PAI scans performed at multiple optical

wavelengths can depict multiple pigments, *e.g.*, hemoglobin and melanin (Oh et al. 2006).

In this article, we describe a prototype PAI system utilizing a focused laser to image *ex vivo* ocular tissues.

METHODS

The PAI system was composed of acoustic and optical subsystems, the photoacoustic assembly and the scanning and data acquisition systems.

Two probe configurations, shown schematically in Figure 2, were fabricated. The first consisted of a custom-made focused 35-MHz single-element polymer US transducer with a 6-mm aperture and 12-mm focal length (Panametrics-NDT, Waltham, MA, USA) and optical axis oriented at a 30-degree angle to the acoustic axis while sharing a common focal point. The second configuration consisted of a custom 20-MHz single-element lithium niobate ring transducer fabricated at the Resource Center for Medical Ultrasonic Transducer Technology, University of Southern California. This probe had a 12 mm outer diameter, 5 mm inner diameter and 30 mm focal length. The optics were inserted through the central aperture of the transducer, allowing coaxial optical and acoustic beams with a common focus (Kong et al. 2009).

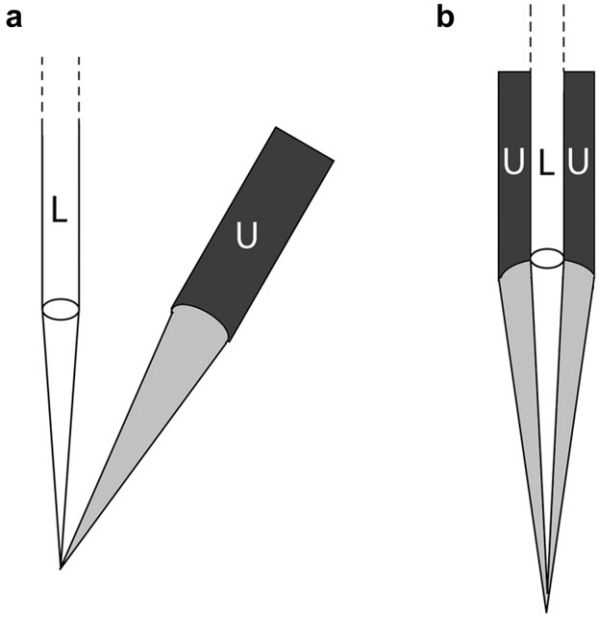

Fig. 2. Schematic drawings of the photoacoustic assemblies. (a) The angled assembly utilized a focused 35-MHz single-element transducer, U. The pulsed laser, L, was introduced using a photonic crystal fiber and focused with a microlens to a point coinciding with that of the ultrasound transducer. (b) The coaxial assembly used a 20-MHz ring transducer, U, with a 5-mm central aperture. Laser pulses were introduced though the central aperture with a photonic crystal fiber and focused with a microlens to a point coincident with the acoustic focus.

The optical system utilized a diode-pumped passively Q-switched Cr,Nd:YAG microchip laser as the irradiation source (Zhou et al. 1993). The laser generated 5-ns pulses at a wavelength of 1064 nm and repetition rate of 500 Hz. The output of the Q-switched laser was then frequency-doubled in a potassium titanium oxide phosphate (KTP) crystal to produce 532-nm pulses. The crystals for the laser and harmonic generation were purchased from Casix, Inc. (Fuzhou, China) and the laser device was developed at Hunter College. With a conversion efficiency of 50%, the energy after the conversion is approximately equally divided in 532 nm and 1064 nm and either wavelength may be selected by a filter. The laser pulses were coupled into to a 2-meter-long photonic crystal fiber (LMA-35 for the angled set-up and LMA-20 for the coaxial setup; NKT Photonics, Birkerod, Denmark). A plano-convex lens was used to project the image of the exit end of the fiber to the focal plane of the transducer. By placing the exit end of the fiber at twice the focal distance in air, the image is formed at two times the focal distance in water with a magnification of 1, producing a laser spot size at the focus equal to the fiber core diameter. The position of the fiber end was adjusted with a three-dimensional (3-D) translational stage to ensure a common focus of the laser and ultrasonic beams. For the angled set-up, the focal length of the imaging lens was 7.5 mm (in air) and the core diameter of the fiber was 35 μm. For the co-axial set-up, the focal length was 12 mm and the fiber core diameter was 20 μm.

The probe was attached to computer-controlled linear stages allowing positioning to a precision of 1 μm in three orthogonal axes. During scanning, the laser emitted pulses at a rate of 500 Hz and the rate of linear motion of the stage was calculated to place vectors at evenly spaced user-specified intervals. Each light pulse was detected by a photodiode and this was used for synchronization.

In PAI mode, the US pulser/receiver (Model 5900; Panametrics-NDT, Waltham, MA, USA) was used as a passive receiver and the photodiode signal was used to trigger the digitizer. In pulse/echo mode, the laser continued to pulse as usual and the photodiode signal was used to trigger both the ultrasound pulser and the digitizer. Ultrasound data were acquired at 12-bit resolution at a sample rate of 400 MHz. In all cases, range between the PAI probe and the tissue under study was adjusted so as to place the region of interest in the focal zone.

The PAI signal appears at one-half the temporal delay of the pulse/echo signal. Since the speed of light is effectively instantaneous, the PAI signal need travel only one-way, while in pulse/echo mode the pulse must travel from the transducer to the tissue and the echoes then travel the same distance back to the transducer. This, in principle, allows PAI and conventional pulse/

echo US data to be acquired simultaneously, although in our experiments we first acquired US and then PAI data to allow optimization of gain and gate settings for each mode.

We first scanned a 12.5 μm thick aluminum wire (Omega Engineering, Stanford, CT, USA) to ascertain lateral resolution in both pulse/echo and PAI modes as a function of range. Scans were acquired at range intervals of 0.25 mm and the 6-dB width of the wire target was measured as well as the 6-dB depth of field.

We then imaged fresh *ex vivo* pig eyes that were obtained from a commercial abattoir. After immersing the whole eye in normal saline solution, we imaged the anterior segment through the cornea. We then cut the globe circumferentially in the region of the pars plana to separate the anterior segment from the remainder of the globe. We removed the vitreous (taking the fragile retina with it) and the lens. We then laid the posterior segment face upwards, scanned and acquired US and PAI data. We then positioned the anterior segment with the internal structures facing upwards and acquired US and PAI data.

RESULTS

For the 35-MHz angled probe, the 6-dB lateral width of the wire target in the focal plane was 90 μm in pulse/echo mode and under 30 μm in photoacoustic mode at 532 nm and 1064 nm. The angled probe had a very limited photoacoustic depth-of-field, measuring about 100 μm, defined by the region in which the laser beam crosses the focal zone of the ultrasound transducer. For the 20 MHz coaxial ring probe, the wire target reflection at the focus was 192 μm in pulse/echo mode. In photoacoustic mode, the width of the wire target was 24 μm at both 532 nm and 1064 nm. For the coaxial probe, the photoacoustic depth-of-field was approximately 5 mm in clear media.

We next obtained photoacoustic and pulse/echo images of *ex vivo* pig eyes. For reference in interpreting photoacoustic images of ocular structures, histologic cross-sections of the anterior segment and posterior of a human eye (similar anatomically to pig) are provided in Figure 3.

Figure 4 shows comparative US and PAI images of the iris obtained using the angled 35-MHz assembly at 1064 nm. While all the anterior segment structures are visualized in pulse/echo ultrasound, only the iris is detected photoacoustically due to the presence of melanin in this structure. US and PAI images of the anterior segment obtained using the coaxial 20-MHz system with a 532-nm pulsed laser are shown in Figure 5. Here, primarily the anterior surface of the iris is seen in the photoacoustic image due to the stronger absorption of light by melanin at this wavelength. Surprisingly, the anterior surfaces of the cornea and crystalline lens are seen. The sharpness of these surfaces appears far superior in the photoacoustic image to that seen in the 20-MHz pulse/echo image.

To rule out the possibility of nonlinear two-photon absorption as the cause of the lens surface signal, we imaged the lens surface at a series of five pulse energies

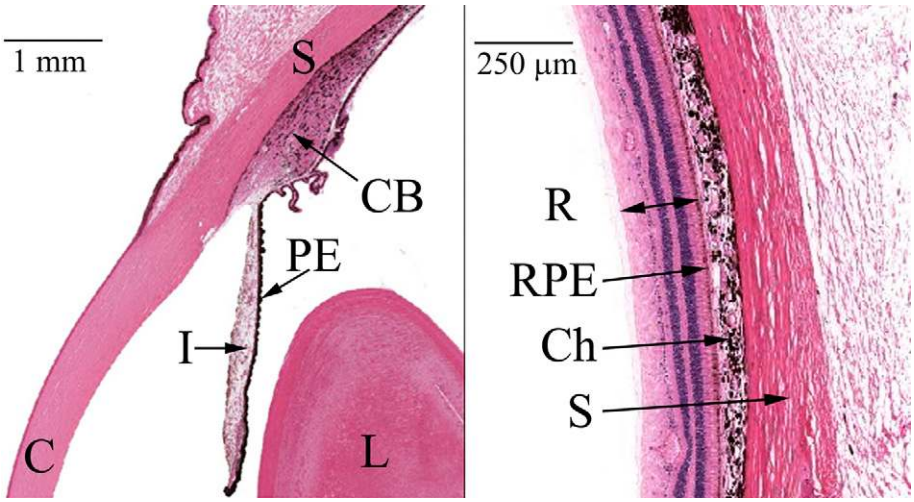

Fig. 3. Histologic sections of human anterior segment (left) and posterior coats (right). The iris, ciliary body and choroid, collectively constituting the uvea, are highly vascular pigmented tissues. The iris pigment epithelium and the retinal pigment epithelium are highly pigmented layers lining the posterior surfaces of the iris and retina respectively. The ciliary processes are arranged in a radial fashion with respect to the pupil. (C = cornea; I = iris; PE = iris pigment epithelium; CB = ciliary body; S = sclera; R = retina; RPE = retinal pigment epithelium; Ch = choroid. Hematoxylin and eosin stain, ×40 original magnification. Histologic section courtesy of Patrice F. Spitalnik MD, Dept. of Pathology, Columbia University Medical Center.)

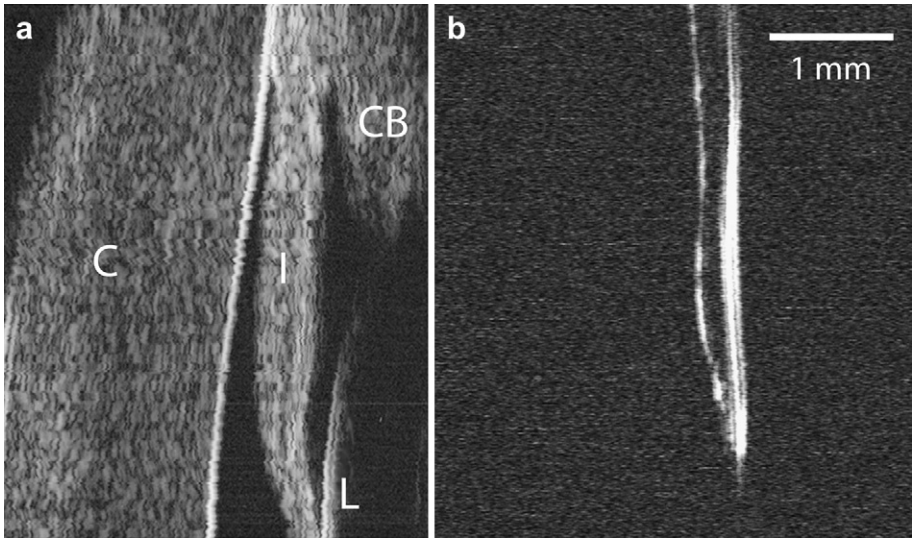

Fig. 4. Comparative images of the anterior segment of an *ex vivo* pig eye performed with (a) 35 MHz pulse/echo ultrasound and (b) by photoacoustic imaging at 1064 nm. In the conventional ultrasound imaging, all anterior segment structures are visualized, including the cornea, C, iris, I, ciliary body, CB and the anterior lens capsule, L. In the photoacoustic image, only the iris, pigmented with melanin, is seen.

ranging from 0.11 to 1.8 μJ at 532 nm. At each pulse energy, we recorded the maximum peak-to-peak voltage of the 50-dB amplified photoacoustic signal from three adjacent vectors at the same position in each scan. We then plotted the mean values of photoacoustic amplitude against laser pulse energy and determined the correlation coefficient. Results, shown in Figure 6, demonstrated a linear relationship ($R^2 = 0.987$).

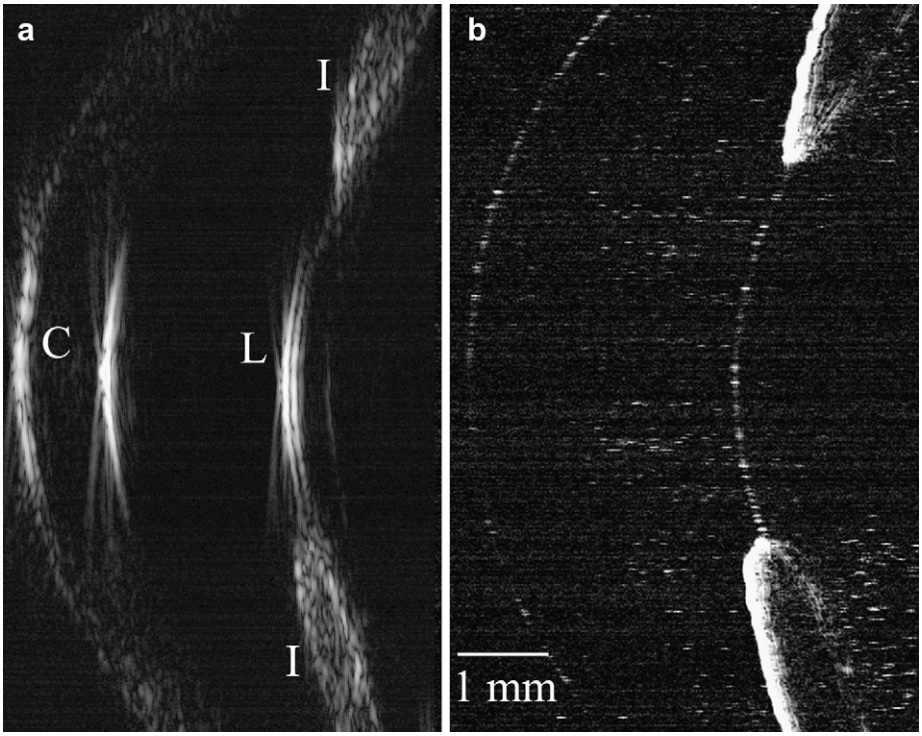

Fig. 5. Pulse/echo (a) and 532-nm photoacoustic image (b) of anterior segment of *ex vivo* pig eye obtained using 20-MHz probe with coaxial optics. The pulse/echo image shows reflections from the specular corneal (C) surfaces and that of the lens (L), as well as backscatter from the iris (I). The pigmented iris absorbs light and hence is visible photoacoustically. The anterior surfaces of the cornea and the lens both produce photoacoustic signals. Also present in the photoacoustic image are semi-random signals appearing a few microseconds after large acoustic emissions, possibly due to collapse of microbubbles.

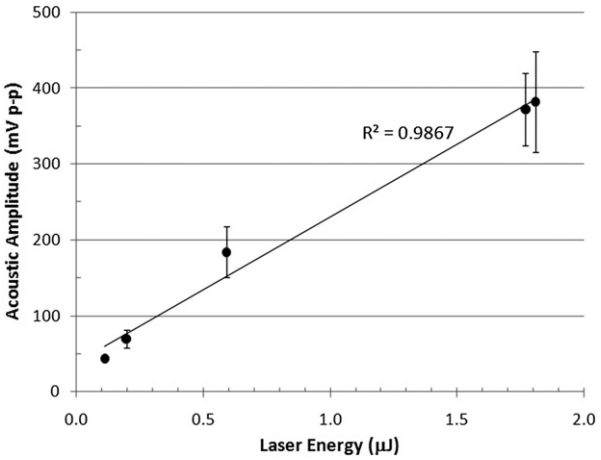

Fig. 6. Plot of peak-to-peak voltage of ultrasound signal from surface of lens versus laser pulse energy as measured at fiber tip. Linear relationship indicates that this signal originates from conventional optical absorption rather than nonlinear process such as two-photon absorption. Error bars represent 95% confidence bounds.

Photoacoustic and US images of the excised posterior of the eye are shown in Figures 7 and 8. In Figure 7, the 20-MHz ring transducer with coaxial 532-nm pulsed laser was used for PAI. The pulse/echo US image clearly depicts the choroidal surface and underlying sclera, but due to speckle, the choroidal/scleral interface is hard to discern. The PAI image shows a very sharp depiction of the choroidal surface but with limited penetration due to the strong absorption of the green laser by melanin. Figure 8 presents comparative pulse/echo and photoacoustic images of the choroid obtained at 532 nm and 1064 nm. While the signal-to-noise is lower at 1064 nm, the lower optical attenuation at this wavelength allows clear depiction of both surfaces of the choroid.

The region of the ciliary body was scanned by cutting the eye in half in a coronal section through the pars plana. After removal of the lens, the anterior segment was placed with the internal structures of the anterior segment face-up allowing them to be scanned photoacoustically. Figure 9 shows comparative US and PAI images obtained in a scan plane running perpendicular to the orientation of the ciliary processes. The 20-MHz US image provides very limited diagnostic information but there is some hint of the ciliary body and underlying sclera. The PAI images clearly depict multiple ciliary processes as well as zonular fibers at high-resolution. The bright ''corrugated'' surface underlying the processes is consistent with the anatomy of the iris pigment epithelium.

DISCUSSION

In this article we demonstrated high-resolution PAI of *ex vivo* eyes. We found that images in the NIR provided better penetration than those obtained with the green (532-nm) laser but with reduced sensitivity. PAI images were distinctly different in appearance from those obtained with pulse/echo ultrasound. In pulse/echo ultrasound, significant reflections and backscatter occur in the sclera, iris and choroid and primarily surface reflections from more homogeneous tissues such as the cornea and lens. In contrast, photoacoustic signals were generated primarily by pigmented tissues including the iris, ciliary body and choroid.

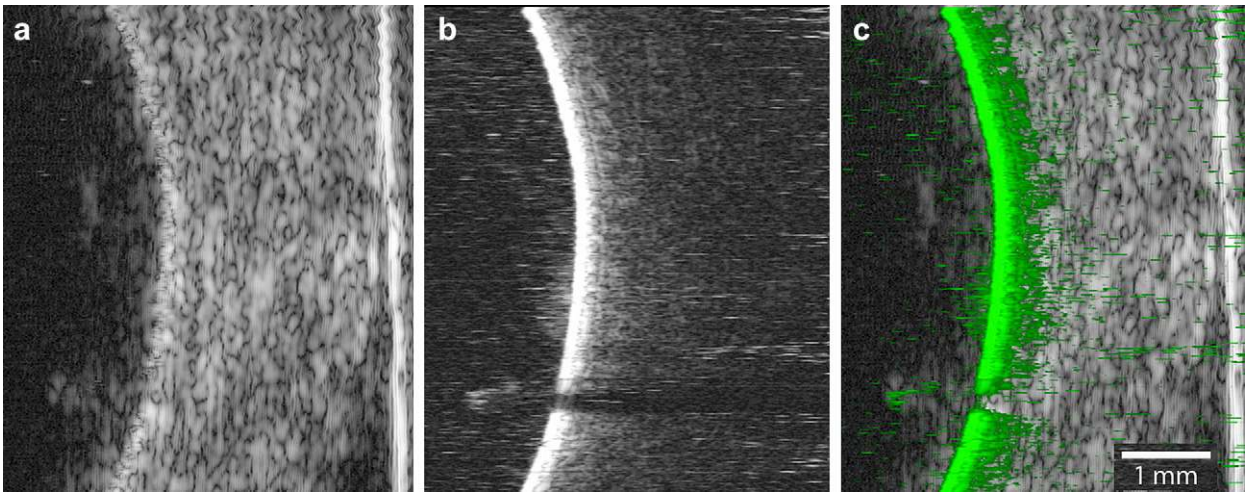

Fig. 7. Pulse/echo (a) and photoacoustic (b) images of the choroid in an *ex vivo* pig eye obtained with the 20-MHz ring transducer using a 532-nm green laser. In pulse/echo mode, the choroidal surface and underlying sclera all produce echoes. In the photoacoustic image, a large signal is generated at the choroidal surface. Note the shadow from debris anterior to the choroidal surface (possibly detached retina). Acoustic signals appear in the photoacoustic image several microseconds after encountering strong absorbance by the choroid. In (c), the photoacoustic data (rendered in green) are superimposed on the gray-scale pulse/echo data to form a fused image.

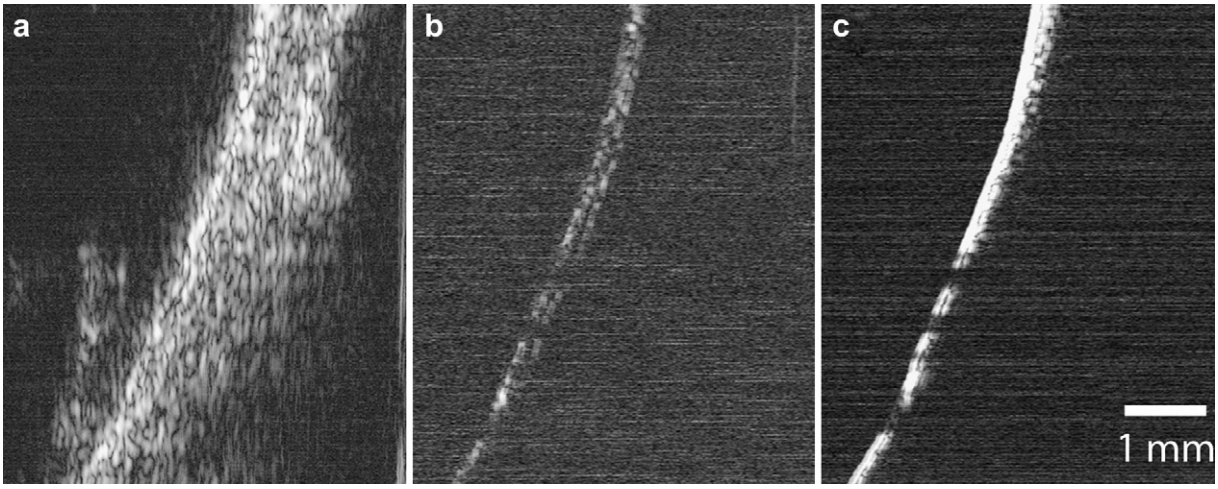

Fig. 8. Pulse/echo images of the choroid of an *ex vivo* pig eye (a) and coregistered photoacoustic images obtained at 532 nm (b) and 1064 nm (c). The 1064-nm near-infrared laser provides better penetration, allowing depiction of the full thickness of the choroid. The 532-nm green laser produces a higher amplitude signal, but also greater absorption and lower penetration than the infrared laser.

Surprisingly given their apparent optically transparency, the anterior lens and corneal surfaces produced PAI signals at 532 nm. We considered two-photon absorption (Shen 1984) as a possible explanation. A chromophore that absorbs in the UV (*e.g.*, at 532/2 = 266 nm) can also be excited by two photons of green (532 nm) visible light that are absorbed nearly simultaneously. Since UV is strongly absorbed, this might have explained the photoacoustic signal from the lens surface. However, the power densities used in our experiment were several orders of magnitude lower than those reported to generate this effect in tissues (Levene et al. 2004), making this mechanism seem unlikely. Furthermore, since two-photon absorption increases quadratically with fluence, our experimental finding of a linear relationship between pulse energy and photoacoustic amplitude (Fig. 6) rules out this mechanism and supports conventional absorption. It is known that some absorption, increasing with age, does occur in the human lens (Ranjan and Beedu 2006). In the pig lens, the fractional absorption at 532 nm is reported to be approximately 0.003 for light traversing its full thickness, indicating that it is quite transparent at this wavelength (Lei and Yao 2006). Lei and Yao (2006), however, also observed higher absorption in lenses from pigmented than from albino mice and suggested that a thin tissue layer at the lens surface might absorb strongly or that an unknown chromophore may be present. Another possibility is that post-mortem changes might have increased surface absorption. Future *in vivo* studies will help clarify the source of this signal.

In the present study, imaging of the choroid and ciliary body were performed by sectioning the eye. This set-up facilitated illumination of these tissues by the pulsed laser and allowed us to avoid attenuation of the ultrasound signal by the crystalline lens, which is a strong acoustic absorber, as well as the optical and acoustic refractive effects of these structures. For PAI of the retina/choroid in intact globes, several potential approaches suggest themselves. First, an angled arrangement between the US probe and the laser would allow the laser to be introduced through the pupil while the acoustic signal would reach the transducer through a path avoiding the lens. Alternatively, a ring-transducer arrangement could allow acoustic attenuation by the lens to be avoided, but a larger inner aperture would be required to avoid the lens, which is approximately 1 cm in diameter. It may also be possible to use a simple coaxial arrangement: because the PAI signal only crosses the crystalline lens in one direction, as opposed to the two-way traversal in pulse/echo ultrasonography, attenuation would be significantly less than that experienced in conventional US. This might allow use of transducer frequencies as high as 20 MHz. However, the cornea and lens also introduce refractive effects on the optical beam, shortening the optical focal length and displacing the optical focal point inwards towards the eye's optical axis when the light beam enters the eye from a non-axial position. Our analyses indicate that these effects can measure in hundreds of microns at the retina, and thus must be compensated for in any focused PAI system's design.

PAI may be of particular value in imaging the eye in small animals, especially in rats and mice, where the sclera may be thin enough (10-20 μm in mice (Demetriades et al. 2008) compared with 500–1000 μm in humans) to allow penetration of light directly through the sclera rather than via the cornea/pupil route.

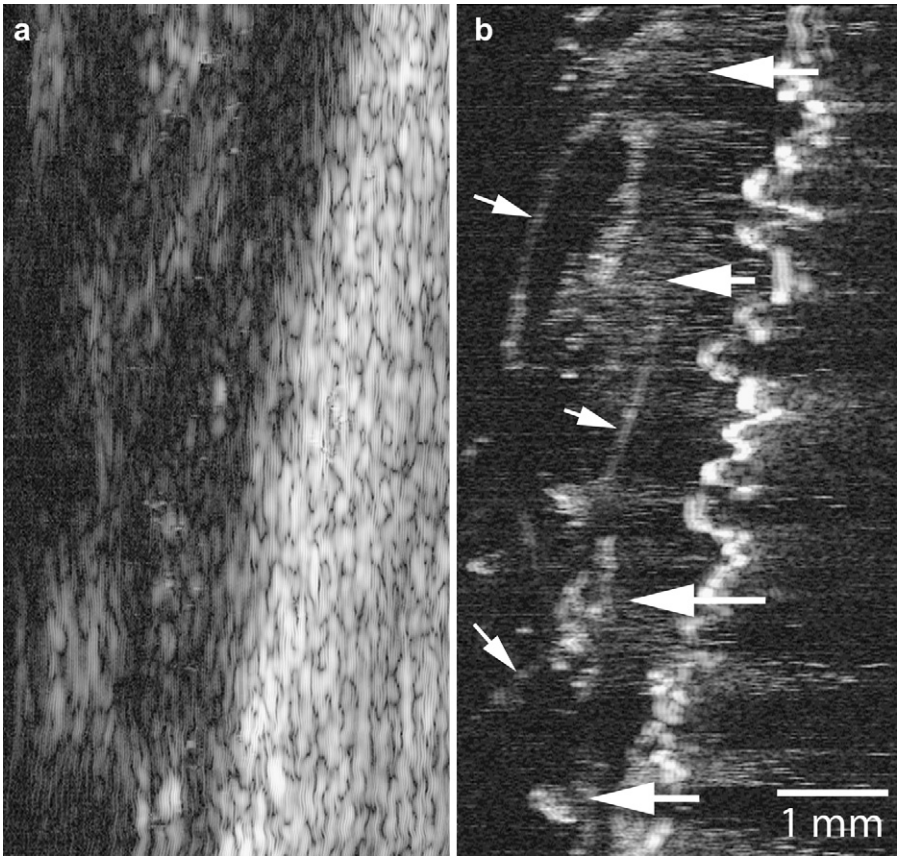

Fig. 9. 20-MHz pulse/echo (a) and 532-nm photoacoustic images (b) of the ciliary body in an *ex vivo* pig eye. These images were obtained by excising the anterior segment with a 360-degree incision in the region of the pars plana. After the vitreous and lens were removed, scans were performed with the internal surface of the iris facing the probe, and in a plane orthogonal to the orientation of the ciliary processes, which are radially arranged with respect to the pupil. The relatively low resolution of the 20-MHz transducer suggests the individual processes but these are clearly visualized in the photoacoustic image (large arrows). Also seen photoacoustically are zonular fibers (thin arrows). The bright, irregular surface seen below the processes is consistent with the ''washboard'' texture of the posterior surface of the iris, which is highly pigmented.

Safety is a major concern in any ophthalmic application of lasers. Under ANSI guidelines (ANSI 2007), for wavelengths in the visible to NIR (400–1400 nm, the ''retinal hazard region''), any point light source is treated as being focused by the cornea and lens to an approximately 20 μm diameter spot on the retina. In our PAI system, the 1-μJ laser beam has a high degree of spatial coherence and must be treated as such a point source. The relevant quantity for ophthalmic safety calculations is the total energy entering the eye through the pupil. If we assume that areas irradiated by consecutive laser pulses in a rapid scanning system do not overlap, the single-exposure maximum permissible exposure (MPE) standard is applicable. For a laser beamwidth smaller than the maximum pupil aperture, the energy must be averaged over the pupil area for comparison with the MPE (Sliney and Wolbarsht 1980). The 1-μJ pulse energy of our system averaged over a dilated pupil of 7 mm diameter is 2.56 μJ/cm^2, which is a factor of 10 larger than the MPE of 0.25 μJ/cm^2 at 532 nm for a 5-ns pulse and approximately equal to the MPE of 2.5 μJ/cm^2 at 1064 nm. We deem these levels to be acceptable for the preliminary feasibility studies described in this report. Since the PAI signal, especially at 532 nm, was quite high, in fact exceeding the pulse/echo signal in magnitude in some instances, we are confident that power densities compliant with ophthalmic ANSI standards will be practicable.

Since our study was restricted to *ex vivo* tissues, hemoglobin was effectively not present leaving melanin as the primary chromophore. In contrast, hemoglobin will be a major chromophore *in vivo*. Consequently, potential clinical applications of PAI would include visualization of microcirculation in the retina and choroid in conditions such as macular degeneration and diabetic retinopathy. This, coupled with the ability of PAI to detect melanin, would be useful in evaluation of small melanomas and nevi. Potentially, PAI optical wavelengths suitable for detection of pathology-associated pigments

such as lipofuscin (absorbing in the blue) could be performed. Imaging of deoxyhemoglobin might allow detection of regions of ischemia or anoxia in tumors and the optic nerve in glaucoma.

Use of a focused light source necessitates data acquisition serially, one vector at a time. While the present setup utilized relatively slow linear stages and laser pulse rates for scanning, requiring over one-second per scan plane, much higher speeds can be realized even with mechanically scanned systems. Though real-time imaging can be performed by combining a linear array with an unfocused pulsed laser (Kolkman et al. 2008), such systems would lack the enhanced resolution obtained by use of a focused light source as described in this report. The ultimate goal would be development a high-speed high-resolution PAI system for 3-D imaging of the region of the macula, as is now performed with OCT (de Bruin et al. 2008).

The fovea, located in the center of the macula and the seat of sharp central vision, is routinely imaged in OCT. Because it measures just 1 mm in diameter by 120 μm in depth (Atchison et al. 2006), it cannot generally be visualized with pulse/echo ultrasound. The use of a focused laser as detailed in this study may allow PAI to resolve this clinically important structure, especially if PAI, as is generally the case with ophthalmic OCT scanners, could be coupled with scanning laser ophthalmoscopy to provide simultaneous real-time imaging of the retinal surface. Furthermore, because PAI is not dependent upon ballistic photons as is OCT, it will have the potential to image to greater depths, offering improved depiction of the choroid, which is poorly visualized with OCT.

CONCLUSION

PAI is an imaging modality that detects optical absorption and is, thus, independent of tissue properties detected by conventional pulse/echo ultrasound and OCT. Because PAI can be performed simultaneously with conventional pulse/echo ultrasound, these modalities can be readily combined in image fusion. For the thin tissue layers of the eye, the use of a focused laser may provide sufficient resolution to visualize structures such as the fovea that are beyond the resolution capabilities of pulse/echo ultrasound and because of its lack of dependence on ballistic photons, it may offer improved penetration compared to OCT.

Acknowledgements—Supported in part by grant UL1 RR024996 of the Clinical and Translational Science Center at Weill Cornell Medical College, the Biomedical Engineering Research Fund of the Riverside Research Institute, the Dyson Foundation and grant RR03037 from the National Center for Research Resources, a component of the NIH.

REFERENCES

American national standard for safe use of lasers ANSI Z136.1-2007. Orlando: Laser Institute of America; 2007.

Atchison D, Lucas SD, Ashman R, Huynh MA, Schilt DW, Ngo PQ. Refraction and aberration across the horizontal central 10° of the visual field. Optom Vis Sci 2006;83:213–221.

de Bruin DM, Burnes DL, Loewenstein J, Chen Y, Chang S, Chen TC, Esmaili DD, de Boer JF. *In vivo* three-dimensional imaging of neovascular age-related macular degeneration using optical frequency domain imaging at 1050 nm. Invest Ophthalmol Vis Sci 2008;49: 4545–4552.

Demetriades AM, Deering T, Liu H, Lu L, Gehlbach P, Packer JD, MacGabhann F, Popel AS, Wei LL, Campochiaro PA. Trans-scleral delivery of antiangiogenic proteins. J Ocular Pharm Ther 2008;24: 70–79.

Drexler W, Fujimoto JG. State-of-the-art retinal optical coherence tomography. Prog Ret Eye Res 2008;27:45–88.

Emelianov SY, Aglyamov SR, Shah J, Sethuraman S, Scott WG, Schmitt R, Motamedi M, Karpiouk A, Oraevsky AA. Combined ultrasound, optoacoustic and elasticity imaging. Proc SPIE 2004; 5320:101–112.

Hammer M, Roggan A, Schweitzer D, Muller G. Optical properties of ocular fundus tissues–An *in vitro* study using the double-integrating-sphere technique and inverse Monte Carlo simulation. Phys Med Biol 1995;40:963–978.

Huang D, Swanson EA, Lin CP, Schuman JS, Stinson WG, Chang W, Hee MR, Flotte T, Gregory K, Puliafito CA, Fujimoto JG. Optical coherence tomography. Science 1991;254:1178–1181.

Ishikawa H, Schuman JS. Anterior segment imaging: Ultrasound biomicroscopy. Ophth Clin North Am 2004;17:7–20.

Kolkman RGM, Brands PJ, Steenbergen W, van Leewen TG. Real-time *in vivo* photoacoustic and ultrasound imaging. JBO Lett 2008;13. 050510-1–3.

Kong F, Chen Y-C, Lloyd HO, Silverman RH, Kim H, Cannata JM, Shung KK. High-resolution photoacoustic imaging with focused laser and ultrasonic beams. Appl Phys Lett 2009;94:033902-1-3.

Kruger RA. Photoacoustic ultrasound. Med Phys 1994;21:127–131.

Lei B, Yao G. Spectral attenuation of the mouse, rat, pig and human lenses from wavelengths 360 nm to 1020 nm. Exp Eye Res 2006; 83:610–614.

Levene MJ, Dombeck DA, Kasischke KA, Molloy RP, Webb WW. *In vivo* multiphoton microscopy of deep brain tissue. J Neurophysiol 2004;91:1908–1912.

Maslov K, Zhang HF, Hu S, Wang LV. Optical-resolution photoacoustic microscopy for *in vivo* imaging of single capillaries. Opt Lett 2008; 33:929–931.

Oh J-T, Li M-L, Zhang HF, Masloff K, Stoica G, Wang LV. Three-dimensional imaging of skin melanoma *in vivo* by dual-wavelength photoacoustic microscopy. J Biomed Opt 2006;11. 034032-1–4.

Oraevsky AA, Karabutov AA. Optoacoustic tomography. In: Vo-Dinh T, (ed). Biomedical photonics handbook. Vol. PM125, Chapter 34. Boca Raton, FL: CRC Press; 2003. 34/1–34/34.

Oraevsky AA, Jacques SL, Esenaliev RO, Tittel FK. Laser based optoacoustic imaging in biological tissues. Proc. SPIE 1994;2134A: 122–128.

Oraevsky AA, Jacques SL, Tittel FK. Determination of tissue optical properties by time-resolved detection of laser-induced stress waves. Proc SPIE 1993;1882:86–101.

Ranjan M, Beedu SR. Spectroscopic and biochemical correlations during the course of human lens aging. BMC Ophthalmol 2006;6:1–9.

Rovati L, Cattini S, Zambelli N, Viola F, Staurenghi G. *In vivo* diffusing-wave-spectroscopy measurements of the ocular fundus. Opt Expr 2007;15:4030–4038.

Sardar DJ, Mayo ML, Glickman RD. Optical characterization of melanin. J Biomed Opt 2001;6:404–411.

Shen YR. The principles of nonlinear optics. New York: Wiley-Interscience; 1984.

Silverman RH. High resolution ultrasound imaging of the eye. J Clin Exp Ophthalmol 2009;37:54–67.

Sliney D, Wolbarsht M. Safety with lasers and other optical sources. New York: Plenum Press; 1980.
Tuchin V. Tissue optics. Light scattering methods and instruments for medical diagnosis. 2nd ed. Bellingham, WA: SPIE Press; 2007.
Wray S, Cope M, Delpy DT, Wyatt JS, Reynolds EOR. Characterization of the near infrared absorption spectra of cytochrome aa_3 and haemoglobin for the non-invasive monitoring of cerebral oxygenation. Biochim Biophys Acta 1988;933:184–192.
Xu M, Wang LV. Photoacoustic imaging in biomedicine. Rev Sci Instr 2006;77. 041101–1–21.
Zhou S, Lee KK, Chen YC, Li S. Monolithic self-Q-switched Cr, Nd:YAG laser. Opt Lett 1993;18:511–513.